Paper

Mechanical and Architectural Changes in Animal Bone Following Fast Neutron Irradiation

Eduardo Galiano, Jinlu Liu, Beide Ren, and Penghao Xu[1]

Abstract—**Damage to healthy bone following exposure to ionizing radiation has been well documented for at least seven decades. Among the reported effects are a transient increase in stiffness and a reduction in breaking strength. These changes have been linked to a decrease in osteoblast proliferation and differentiation, inducing cell cycle arrest, reducing collagen production, and increasing sensitivity to apoptotic agents. In this work, we analyzed some mechanical and structural changes in compact costal bovine bone (Hereford breed, n = 9) subjected to escalating doses of fast neutrons from a ^{7}Li(p, n)^{7}Be reaction. The mean neutron energy was 233 keV with calculated absorbed doses ranging from 0 to 4.05 ± 10% Gy. Samples were subjected to Young's Modulus (YM) and breaking strength testing with a Universal Testing Machine (UTM). We found an increase in Young's Modulus and a decrease in breaking strength as functions of increasing dose equivalent. Optical coherence tomography (OCT) revealed trabecular displacement into compact bone in an irradiated sample (D = 4.05 ± 10% Gy), with breaching of the endosteal wall. OCT further revealed a "crack-like" structure across the irradiated sample, potentially consistent with damage from a proton track resulting from an elastic (n,p) reaction. No previous report has been found on mechanical changes in large mammalian bones following fast neutron doses, nor of the OCT imaging of such samples.**

Health Phys. 127(2):298–305; 2024

Key words: bones; human; dose; bone; neutrons; radiation; medical

INTRODUCTION

Damage to healthy bone following radiation therapy increases the risk of fracture among long-term cancer survivors. For example, women treated for various pelvic tumors have been shown to have a greater than 65% increased incidence of hip fracture 5 y after treatment (Wiley et al. 2011). Another scenario—for which there is limited understanding—is the potential long-term negative impact on skeletal health associated with extended spaceflight. This is a relevant consideration, given the political commitments that several nations (i.e., China, India, the Russian Federation, the EU, and the US) have made to send human expeditions to Mars within the next 20 to 30 y (Lang et al. 2004). The absorbed doses for a proposed 2-y expedition are not insignificant; the estimated tissue dose equivalent rates (from cosmic radiation) are between 1.0 to 2.5 mSv d^{-1}, with a significant fraction due to fast neutrons from inelastic proton scattering in spacecraft structural components (NCRP 2000). This excludes an additional estimated dose equivalent of 1.0 to 2.0 Sv that a solar particle event or "solar flare" lasting 8 to 24 h would contribute.

In healthy animal bones irradiated to such doses, trabecular enlargement has been reported (Wlliams et al. 2006). Nyaruba et al. reported a significant loss in stiffness (increased elasticity) in rodent bones exposed to high doses of x-rays but found no change in breaking strength (Nyaruba et al. 1998). Mitchell and Logan reported significant loss of trabecular architecture in the bones of patients receiving photon radiotherapy (Mitchell and Logan 1998). In terms of loss of mechanical integrity of bone in mice following irradiation, Alwood and collaborators reported that a 2.0 Gy dose of heavy ions caused a loss of vertebral stiffness as tested by compression loading (Alwood et al. 2010), and Wernle et al. reported a reduction of breaking strength (in compression) of femora following a 12.0 Gy dose of x rays (Wernle et al. 2010). Very recently, Wei et al. reported a reduction in the breaking strength (in compression) of the tibia in Sprague-Dawley rats exposed to 7.0 Gy of absorbed dose of x rays with E_{eff} ~ 53 keV (Wei et al. 2023).

From a mechanistic point of view, it has been proposed that x rays cause mechanical and architectural changes in bone by decreasing osteoblast proliferation and differentiation, inducing cell cycle arrest, reducing collagen production and increasing sensitivity to apoptotic agents (Gal et al. 2000). Halliwell and collaborators reported that approximately two-thirds of the radiation damage to DNA in mammalian osteocytes is caused by the hydroxyl radical as it

[1]Department of Physics and Astronomy, McMaster University, Hamilton, ON L8S 4L8, Canada.

For correspondence contact: Eduardo Galiano, 232 Ottawa St. South, Apt. 2, Hamilton, ON L8K 2E8, Canada, or email at **egalianoriveros@laurentian.ca**.

(*Manuscript accepted* 2 *January* 2024)
0017-9078/24/0

DOI: 10.1097/HP.0000000000001811

reacts amply with ubiquitous organic molecules found in the hydroxyapatite matrix (Halliwell et al. 2021). Osteoradiogenic effects are, however, at least partially reversible. For example, Wei and collaborators recently demonstrated that cerium oxide not only retards loss of bone architecture and strength following x-ray absorption but in fact promotes de novo osteogenesis (Wei et al. 2023).

The most important mechanism by which fast neutrons transfer energy to tissue is through elastic collisions with hydrogen nuclei. This is because hydrogen is the most abundant element in tissue—and in such collisions, half of the incident neutron energy is transferred to the recoiling hydrogen nuclei, as given by the equation:

$$E_{tr} = \frac{2E_0 M_T m_n}{(M_T + m_n)^2}, \quad (1)$$

where E_{tr} is the mean energy transferred, E_0 is the incident neutron energy, M_T is the mass of the target nucleus, and m_n is the neutron mass (Martin 2006). Therefore, the heavier the recoiling nucleus, the less efficient the transfer of energy. For example, in the cases of carbon, nitrogen, and oxygen interactions, only 14%, 12%, and 8% of the incident energy is respectively transferred to the recoiling nucleus. In the unlikely event of a second collision (with a hydrogen nucleus), only 25% of the original incident energy is available for transfer, justifying the validity of First Collision Theory in biomedical applications, such as the present work. More specifically, a 250-keV neutron—the mean energy in our beam—has an absorption coefficient in tissue of approximately 0.2 cm^{-1}, which results in a mean free path of ~5.0 cm (Adair 1950). A relevant question that arises is the extent of the γ dose to tissue in a fast neutron field due to radiative capture (n,γ) reactions within the irradiated tissue itself. Precise measurements at incident neutron energies of 500 keV—energies relevant to the present work—revealed this contribution to be about 1.5% of the total dose (NBS 1957).

These results further justify ignoring this component of the γ dose in overall dose considerations. Furthermore, in fast neutron beams in tissue, kerma, and absorbed dose are essentially indistinguishable given that the range of recoil products (hydrogen or heavier nuclei) is of the order of a micron. Therefore, charged particle equilibrium is rapidly established, and radiative bremsstrahlung losses can be ignored as the cross section for heavy particles is negligibly small. The computed neutron fluence to produce a dose equivalent of 1.0 Sv in soft tissue at 233 keV (mean neutron energy of our beam) is 4.03×10^9 n cm^{-2} (NCRP 1997). In order to compute the corresponding fluence for cortical bone, this soft tissue fluence is multiplied by the (cortical) bone-to-soft tissue neutron kerma ratio at 233 keV:

$$\frac{K_{n,bone@233kev}}{K_{n,soft\ \ tiss@233kev}}, \quad (2)$$

which was reported by Caswell and collaborators as 0.702 (Caswell et al. 1980). The calculated fluence to produce a dose equivalent of 1.0 Sv in (cortical) bone is then 2.83×10^9 n cm^{-2}.

Mechanical changes in animal bones following exposure to ionizing radiation have been reported for at least six decades. However, no reports were found in the literature specifically addressing mechanical or architectural changes in larger mammalian bones exposed to fast neutron fields, which is the question we address in this work. It is a relevant question, considering that fast neutrons can have rather high Q values (~5 to 10) and are insensitive to the protective oxygen effect associated with photons (Hall and Gaccia 2006).

MATERIALS AND METHODS;

In our work, 2.3 MeV protons were incident on a thick lithium target in a $^7Li(p,n)^7Be$ reaction. Its reaction cross section has a threshold at E_p = 1.88 MeV and a broad resonance at 2.2 MeV, which makes it possible to produce ~10^{10} n s^{-1} at moderate proton currents (Liskien and Paulsen 1975). In contrast to other neutron production reactions such as the $^9Be(p,n)$ or $^2H(d,n)$ reactions, the neutron spectrum from the $^7Li(p,n)$ reaction is relatively soft and therefore better suited for the irradiation of biological samples (Kononov et al. 2006). Lee and Zhou reported extensive computational work on this reaction (Lee and Zhou 1998). In essence, they integrated the thick target differential neutron yields over both neutron energy and solid angle to obtain the total neutron yields for the various incident proton energies. For a 2.3-MeV incident proton energy on a thick Li target, they reported a computed neutron yield of 5.78×10^{11} n mC^{-1} of charge deposited on target, with maximum and mean energies of 573 keV and 233 keV, respectively. The broad resonance centered at ~2.2 MeV results in significant gains in both neutron yields and energies. For example, from E_p = 1.90 MeV to 2.30 MeV, neutron yield increases by a factor of 40, and mean neutron energy increases from 38 keV to 233 keV (Matysiak et al. 2011).

Fig. 1 shows a diagram of the target cavity of the McMaster University Tandetron electrostatic accelerator used for this work, located in Hamilton, ON, Canada. The irradiation facility was built for biomedical applications, and detailed descriptions of the design and operating parameters of the accelerator and irradiation cavity have been reported elsewhere (Pejovic-Milic et al. 2006). Fast neutrons are produced via the $^7Li(p,n)$ reaction with $E_p = 2.3 \pm 0.01$ MeV. A Pb filter is positioned upstream of the irradiated specimen

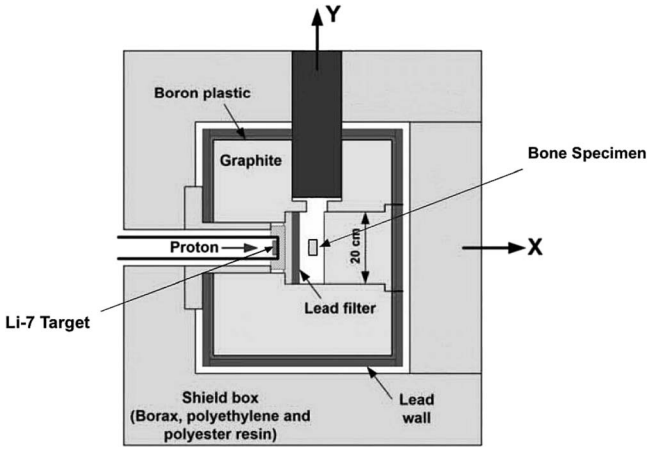

Fig. 1. Diagram of the target cavity of the McMaster University Tandetron electrostatic accelerator (adapted from Byun et al. 2007).

to further reduce the residual γ dose contributed by the competing ^{7}Li(p,p'γ) reaction. Using a tissue-equivalent proportional counter, the neutron absorbed dose in the irradiation cavity has been previously reported (Darvish-Molla et al. 2015). Using Monte Carlo methods, these authors calculated an effective Q value for the neutron field of ~8.5 (E_p = 2.3 MeV), resulting in a reported neutron dose equivalent in soft tissue of 0.9363 ± 10% mSv per μA-min of charge deposited on the Li target. Multiplying by the bone-to-soft-tissue neutron kerma ratio (at 233 keV, the mean neutron energy) of 0.702 (Caswell et al. 1980) results in a neutron dose equivalent per deposited charge (on target) of 0.674 ± 10% mSv/μA-min, for compact (cortical) bone. Furthermore, these authors confirmed the earlier reports that the γ dose for this reaction is ~1% of the neutron dose (Tochilin et al. 1956; NBS 1957).

Power analysis using nine samples in an experimental group results in an approximate confidence level of 93.1% in the detection of a statistically significant change in the mechanical properties of bone exposed to fast neutrons (Bevington and Robinson 2003). This level of confidence was considered satisfactory for the purposes of this work. Bovine Hereford breed costal bone samples were harvested from commercially available, human-consumption-approved meat samples purchased at a local grocer in the Hamilton, ON, Canada area. All samples were initially baked at 200 °C for 60 min. The tissue samples were mechanically deboned and re-baked at 400 °C for 1 h, followed by oven drying at 65 °C for 48 h, and varnishing—a commonly used preparation technique for bony specimens (Kim et al. 2004). Nine samples from two adjacent costal (rib) bones were machined to approximately 3.0 cm × 3.0 cm in frontal area and 2.0 cm in width using a Dremel moto tool (Dremel Model 4300-9/64 High Performance Variable Speed Rotary Tool; Dremel Inc., Racine, WI). A special balsa wood jig was built to support the samples during irradiation. One control sample received zero radiation dose. All irradiations were carried out at the McMaster University electrostatic Tandetron accelerator (Van de Graaf 3.0 MV model KN3000, HVEC; Amerstfoord, The Netherlands). The other eight samples were subjected to 1.0 min, 3.0 min, 5.0 min, 7.0 min, 9.0 min, 11.0 min, 13.0 min, and 15.0 min of beam time (±2.0 s) at a proton current of 400 μA and a beamline pressure of 3.0 × 10^{-7} Torr. Induced activities producing up to ~2,000 cpm 1.0 cm from the samples were recorded. All irradiated samples were allowed to cool down for 24 h before proceeding with mechanical measurements.

Young's Modulus (YM) is a physical parameter that quantifies the elasticity of a solid. It is formally defined as the ratio of the solid's stress to its strain, under a progressively applied compressive—or tensile—load. It is the physical analogue of Hooke's constant for a spring, applied to a solid (Zinke-Allmang et al. 2017). Breaking strength (BS) is the minimum axial force required to induce mechanical failure of the solid, and clearly its measurement is destructive in nature. It is common practice in the engineering testing of materials to acquire YM and BS data simultaneously using a Universal Testing Machine (UTM). This machine consists of a hydraulic piston that compresses (or stretches) the sample at a carefully controlled rate, recording sample compression and applied force up to the point of failure. Based on sample geometry, stress-strain data are generated, and Young's Modulus is extracted by a "best-fit of the slope" algorithm (Galiano and Lapointe 2019). The machine automatically produces a stress-strain curve, a best fit value of YM (in metric units of MPa), and a breaking strength (BS) value (in metric units of N). All samples (n = 9) were subjected to destructive compressional YM and BS measurements along the longitudinal cortical axis with a 500 kN machine (MTS Criterion Series 40 Electromechanical Universal Testing Machine; MTS, Eden Prairie, MN). Fig. 2 illustrates a bone sample undergoing compressional testing in the UTM. During testing, one of the bovine samples was accidentally destroyed before useful data could be generated; therefore, data were only generated for eight samples. As an expected outcome of this type of testing, all samples were destroyed in the process, and therefore this was the last procedure requiring pristine samples in our investigations. Subsequent microscopy work was performed with remaining fragments of the samples.

Optical coherence tomography (OCT) is a recently introduced interferometric tomographic imaging technique using visible—or near visible—wavelengths. Due to its interferometric nature, it is inherently non-diffraction limited. Therefore, it achieves submicron resolution comfortably, approaching that of conventional electron microscopy (Bizheva et al. 2017). The use of relatively long wavelength light allows it to sample much deeper inside the specimen than comparable conventional techniques such as optical

Fig. 2. Bone sample undergoing compressional testing on the UTM. Note the use of acrylic shield to protect personnel from possibility of explosive structural failure of specimen!

confocal microscopy or scanning/tunneling electron microscopy (Harper et al. 2018). OCT imaging of two samples was undertaken; a control sample that received zero dose, and an experimental sample that received a maximum dose corresponding to 15.0 min of beam time (D = 4.05 ± 10% Gy). Imaging parameters were the following: effective focal length = 33.0 mm; working distance = 25.1 mm; image size 1,500 × 500 × 349 pixels in x, y, and z axes, respectively; FOV = 3.00 × 1.00 × 1.20 mm in x, y, and z axes, respectively; and voxel size of 2.00 × 2.00 × 3.43 nm in the x, y, and z axes, respectively. The apparatus with a specimen undergoing imaging is shown in Fig. 3 (OCT Telesto Series TEL221PS; Thorlabs, Newton, NJ).

RESULTS

All numerical data are presented as mean ± standard deviation. Statistical analysis was carried out using GraphPad Prism (version 8.0), and groups were compared using one-way analysis of variance (ANOVA) and a post-hoc Mann Whitney U test. P values < 0.05 were considered significant, consistent with generally accepted standards in biomedical statistical treatments (Bevington and Robinson 2003).

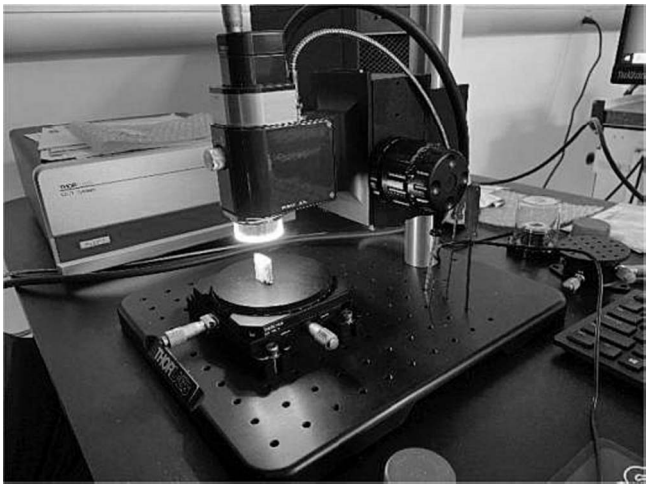

Fig. 3. Bone specimen undergoing imaging in OCT apparatus.

Multiplying the 400 μA beam current by the bone neutron equivalent dose conversion factor of 0.674 ± 10% mSv/μA-min (Davish-Molla et al. 2015; Caswell et al. 1980) results in calculated absorbed doses (multiplied by an RBE or Q factor of 8.5) of 0.28 Gy, 0.81 Gy, 1.89 Gy, 2.48 Gy, 3.07 Gy, 3.51 Gy, and 4.05 Gy for 1.0 min, 3.0 min, 7.0 min, 9.0 min, 11.0 min, 13.0 min, and 15.0 min of beam time exposure, respectively (all doses ±10%).

A representative compressional stress-strain curve is presented in Fig. 4—specifically that of the control sample (zero dose). Note the highly linear strain ($r^2 = 0.9799$) with respect to the applied stress in the 0.5 mm to 0.9 mm range, with some evidence of initial molecular "slipping" in the hydroxyapatite crystal at an applied force of 20 kN, corresponding to a strain (compression) ~0.95 mm. Sudden and complete failure occurs at ~22 kN of applied force at a strain level of ~1.1 mm. Other samples of bovine bones exhibited generally similar stress/strain behavior.

In Fig. 5, Young's Modulus vs. dose for all samples (n = 8) is presented. There is a generally increasing stiffness in bone as a function of dose. A linear-least-squares fit reveals substantial scatter ($r^2 = 0.11$) with small uncertainties; all error bars are contained within the data points. The experimental error for each data point is taken as the measurement accuracy of the UTM, as stated by the manufacturer. These measurements are consistent with results reported by Wernle et al. (2010), who reported a transient increase in stiffness of distal femora in mice within 2 wk following 5.0 and 12.0 Gy single fraction x-rays doses. The investigators proposed that this transient effect is associated with an observed initial increase in cortical volume concurrent with significant ablation of trabecular components. The effect was completely reversed by 12 wk post irradiation

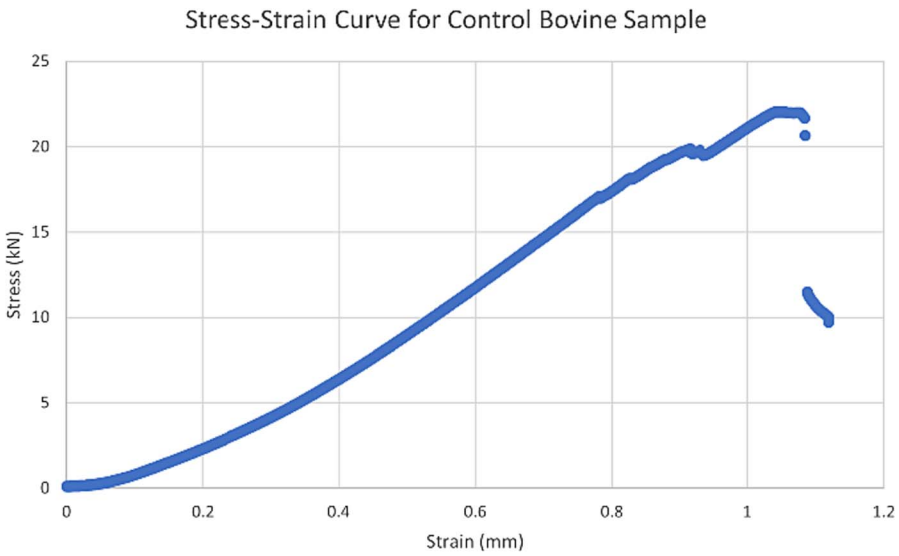

Fig. 4. Stress-strain curve for control sample (zero dose). Complete and sudden failure occurs at ~22 kN of applied force.

(Wernle et al. 2010). In Fig. 6, the breaking force vs. dose for the samples is presented. A least-squares fit reveals a generally decreasing breaking strength with increasing dose, with reasonable scatter for biomedical data ($r^2 = 0.39$; Frost 2020). Again, the uncertainties are small, with the error bars fitting within the data points. A reduction in breaking strength as a function of increased photon dose in mice has been well documented over the course of at least two decades (Nyaruba et al. 1998; Gal et al. 2000; Wernle et al. 2010; Wiley et al. 2011; Halliwell et al. 2021; Wei et al. 2023). No reports were found in the literature regarding the effects of fast neutrons on stiffness or breaking strength in bones of larger mammals.

Micron resolution axial 1.0-mm × 3.0-mm tomographic OCT scans of the endosteal wall separating cortical from trabecular bone of the control sample (zero dose), and a 15-min beam time experimental sample (D = 4.05 ± 10% Gy) are presented in Fig. 7a and b, respectively. In the control sample, the integrity of the endosteum (diagonal linear structure from upper left to lower right) appears conserved, consistent with normal endosteal architecture. In the experimental sample, the integrity of the wall is breached to such an extent that at least one trabecula has been physically displaced into compact bone. The extent of the breach of the endosteal wall is better appreciated in the sagittal plane. Fig. 8a and b are deep sub-micron sagittal tomographic scans of the endosteal walls of the control and experimental samples, respectively. The extent of the breach of the wall and the trabecular displacement are evident. Two reports were found in the literature suggesting the theoretical

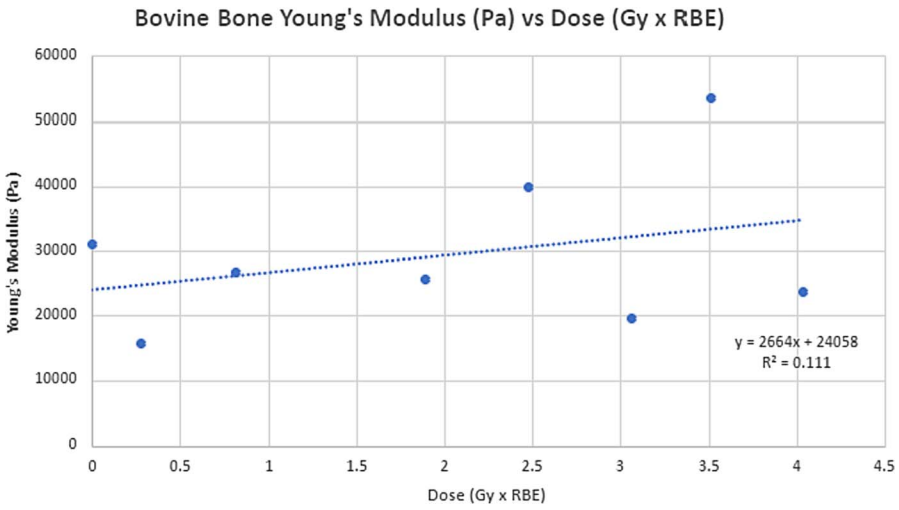

Fig. 5. Young's Modulus vs. dose for samples (n = 8). Note increasing stiffness in bone as a function of dose equivalent. Assumed RBE = 8.5. Error bars contained within the data points.

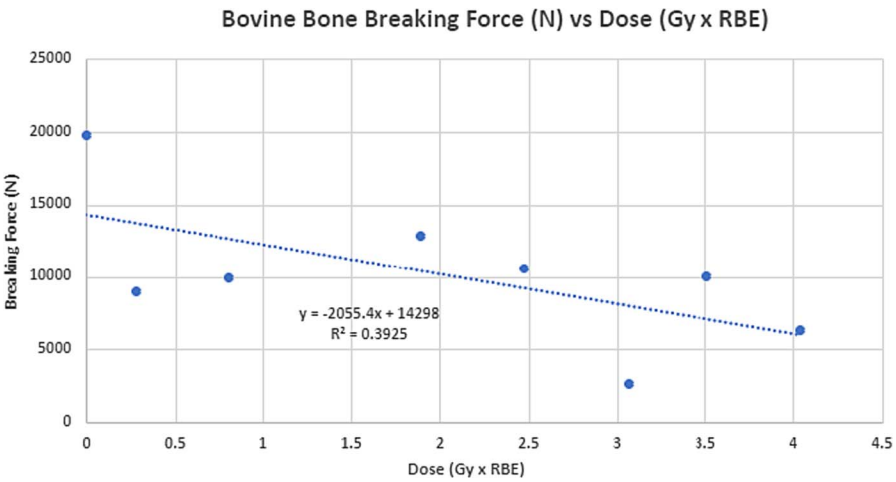

Fig. 6. Compressional breaking force vs. dose for samples (n = 8). Note generally decreasing breaking strength as a function of dose equivalent. Assumed RBE value = 8.5. Error bars contained within the data points.

possibility of trabecular displacement into compact bone, both based on mathematical models of mechanical loading of bones (Ladd et al. 1998; Burr et al. 2002). However, no experimental reports of trabecular displacement of this type following fast neutron irradiation were found.

A deep, sub-micron resolution, three-dimensional volumetric reconstruction of the cortical region of the same experimental sample (D = 4.05 ± 10% Gy) is presented in Fig. 9. The image was rotated through a specific angle to highlight the linear "crack-like" structure across the sample, potentially consistent with damage from a proton track resulting from an elastic (n,p) reaction. The suggestion is plausible given the approximate 2 μm range of a 200-keV proton (roughly the mean neutron energy in our beam) in compact bone (Berger et al. 2017). No such crack-like structures were found in the control sample. Electron photomicrography of proton tracks in biological samples has been previously reported (Fokas et al. 2009). However, no reports of OCT imaging of proton damage in biological samples were found in the literature.

DISCUSSION

In this initial work, which is limited in scope, we report on some mechanical and architectural changes in bovine costal bone samples exposed to a fast neutron field. Among these, we report an increase in the stiffness of cortical bone as quantified by the Young's Modulus within days (n ≤ 7) following irradiation of the samples. A comparable transient increase in bone stiffness in rodents following photon doses has been reported (Wernle et al. 2010). However, no reports were found on the effects of fast neutrons on bone elasticity in animals. The effect is transitory, with a reported reversion interval of 12 wk. It has been proposed that this transient effect may be associated with an observed initial increase in cortical volume despite significant ablation of trabecular components (Wernle et al. 2010). We also report an overall reduction in the compressional failure (or breaking) strength as a function of increasing dose in our samples, generally consistent with previous reports of decreasing breaking strength in rodent bones with increasing photon doses (Nyaruba et al. 1998; Gal et al. 2000; Wernle et al. 2010;

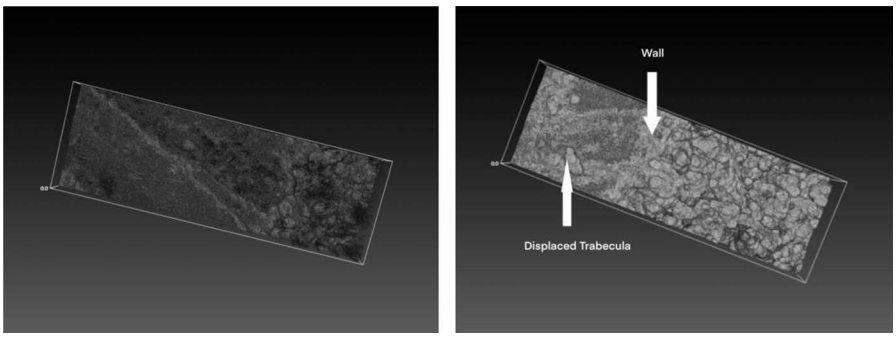

Fig. 7. Left and right, respectively: (a) Axial OCT scans of the endosteal wall of control sample (zero dose), and (b) a 15-minute beam time (D = 4.05 ± 10% Gy) experimental sample respectively. Note loss of wall integrity in the experimental sample, with evidence of trabecular displacement into compact bone.

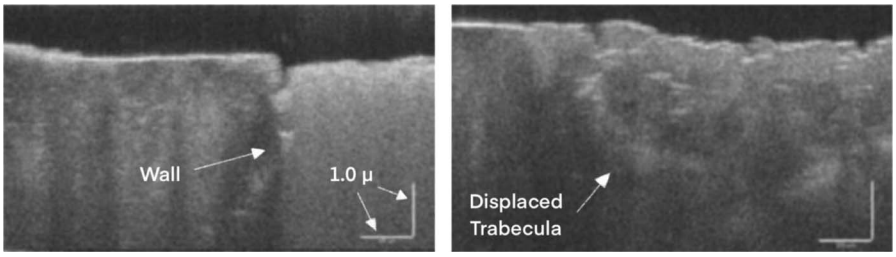

Fig. 8. Left and right, respectively: (a) Submicron endosteal wall sagittal OCT scans of control (left) and (b) experimental (right) samples. In the control sample, lighter region to the right is trabecular bone, darker region to the left is compact (cortical) bone. Note the relative integrity of the vertical boundary between the two regions. Image on right is experimental sample (D = 4.05 ± 10% Gy). Note loss of integrity of the boundary, with trabecula clearly breaching the boundary and projecting into compact (cortical) bone.

Wiley et al. 2011; Halliwell et al. 2021; Wei et al. 2023). No previous reports were found on the effects of fast neutrons on breaking strength in animal bones.

Optical coherence tomography (OCT) scans and derived volumetric reconstructions of the samples are presented. In particular, tomographic evidence of trabecular displacement into compact bone following fast neutron dose is presented. A scan of a crack-like structure in the sample that absorbed the highest equivalent dose (D = 4.05 ± 10% Gy) consistent with a possible recoil proton damage track is presented. No such structure was observed in the control (zero dose) sample. Electron photomicrography of proton tracks in biological samples has been previously reported (Fokas et al. 2009). However, no reports were found of OCT imaging of mammalian bones irradiated with fast neutrons.

In evolutionary terms, costal bones were not adapted to offer resistance to compressional loads; rather, their adaptive pathway optimized resistance to shearing loads to protect inner thoracic organs such as the heart and lungs. In this work, we did not test for changes in the shear moduli of the samples, a physiologically relevant parameter. In our work, the number of samples analyzed was limited (n = 9); therefore, follow-up work with larger numbers of samples is warranted. We are presently extending our work to porcine (Yorkshire breed) costal bones and shall report our observations at a future date.

We underscore that the manufacturer-quoted instrumental uncertainty (or experimental error) for a specific measurement on the UTM only refers to the uncertainty of the given data point. This is not equivalent to the uncertainties in either Young's Modulus or the Breaking Force, which would have required, for example, testing multiple samples from a given bone irradiated to a constant dose, averaging them together, and reporting the standard deviation. An alternative approach would have been to test multiple samples taken from the same bone but from different animals—irradiated to a constant dose—averaging them together and reporting the standard deviation. However, due to budgetary constraints limiting our access to accelerator beam time, we were unable to pursue such strategies. This resulted in a degradation in the statistical power of the results reported in this work.

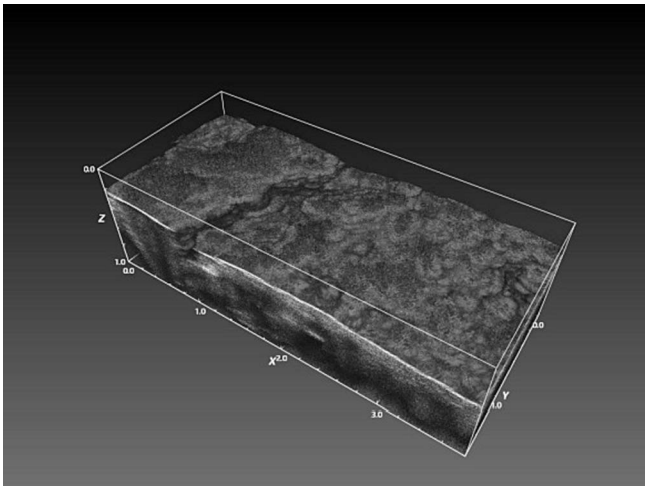

Fig. 9. Sub-micron resolution three-dimensional volumetric reconstruction of compact bone in the experimental sample (D = 4.05 ± 10% Gy). The crack-like structure in the upper left is potentially consistent with damage from a recoil proton resulting from an elastic (n,p) reaction. (units given in μm).

CONCLUSION

A dose-dependent transient increase in stiffness as measured by compressional Young's Modulus, as well as a decrease in compressional breaking strength, are associated with fast neutron doses in the range of 0.28 to 4.05 ± 10% Gy in bovine cortical costal bone. This appears to be the first report on mechanical changes in cortical bone associated with fast neutron dose in large mammals. Trabecular displacement into compact bone is associated with fast neutron dose (D = 4.05 ± 10% Gy), as demonstrated by OCT scanning. No previous reports were found associating this type of trabecular displacement with fast neutron dose. Further, OCT scanning revealed the existence of a crack-like structure in an irradiated sample (D = 4.05 ± 10% Gy), consistent with damage associated with a scattered proton. This appears to be the first report

of OCT analysis of the effects of fast neutron exposure in larger mammalian bones.

Acknowledgments—The authors wish to acknowledge the assistance of Ross Harper, Justin Bennet, and Shereecia Bangura of the Tandetron Accelerator Facility, Duane Lambert of the Health Physics Department, and Joao Firmino of the Centre for Advanced Light Microscopy (CALM), all at McMaster University.

REFERENCES

Adair RK. Neutron cross sections of the elements. Rev Mod Phys 22:249; 1950.

Alwood JS, Yumoto K, Mojarrab R, Limoli CL, Almeida EA, Searby ND, Globus RK. Heavy ion irradiation and unloading effects on mouse lumbar vertebral microarchitecture, mechanical properties and tissue stresses. Bone 47:248–255; 2010.

Berger MJ, Coursey JS, Zucker MA, Chang J. Stopping power & range tables for electrons, protons, and helium ions. Gaithersburg, MD: NIST: NIST Standard Reference Database 124; 2017.

Bevington PR, Robinson DK. Confidence intervals. In: Data reduction and error analysis for the physical sciences. New York: McGraw Hill; 2003: 208–210.

Bizheva K, Tan B, MacLelan B, Kralj O, Hajialamdari M, Denise H, Sorbara L. Sub-micrometer axial resolution OCT for in-vivo imaging of the cellular structure of healthy and keratoconic human corneas. Biomed Optics Express 8:800–812; 2017.

Burr DB, Robling AG, Turner CH. Effects of biomechanical stress on bones in animals. Bone 30:781–786; 1998.

Byun SH, Pejovic-Milic A, McMaster S, Matysiak W, Liu Z, Watters LM, Prestwich WV, McNeill FE, Chettle DR. Dosimetric characterization of the irradiation cavity for accelerator-based in vivo neutron activation analysis. Phys Med Biol 52:1693–1703; 2007.

Caswell RS, Coyne JJ, Randolph ML. Kerma factors for neutron energies below 30 MeV. Radiat Res 83:217; 1980.

Darvish-Molla S, Prestwich WV, Byun SH. Comprehensive radiation dose measurements and Monte Carlo simulation for the ^{7}Li(p,n) accelerator neutron field. Radiat Protect Dosim 171: 421–430; 2015.

Fokas A, Kraftb G, An H, Engenhart-Cabillic R. Ion beam radiobiology and cancer: time to update ourselves. Biochimica et Biophysica Acta 1796:216–229; 2009.

Frost J. R-squared in regression analysis. In: An intuitive guide for using and interpreting linear models. Statistics by Jim Publishing; 2020: 227–229.

Gal TJ, Munoz-Antonia T, Muro-Cacho CA, Klotch DW. Radiation effects on osteoblasts in vitro: a potential role in osteoradio-necrosis. Arch Otolaryngol Head Neck Surg 126:1124–1128; 2000.

Galiano E, Lapointe M. Mechanical, chemical, structural, and radiological changes in pigeon bone, associated with the dietary intake of nickel recovery slag. J Environ Sci Pollut Res 5:348–351; 2019.

Hall E, Giaccia A. Oxygen effects and reoxygenation. In: Radiobiology for the radiologist. Philadelphia, PA: Lippincott Williams & Wilkins; 2006: 85–106.

Halliwell B, Adhikary A, Dingfelder M, Dizdaroglu M. Hydroxyl radical is a significant player in oxidative DNA damage in vivo. Chem Soc Rev 50(15); 2021.

Harper D, Augustin M, Lichtenegger A, Eugui P, Reyes C, Glösmann M, Hitzenberger CK, Baumann B. White light polarization sensitive optical coherence tomography for submicron axial resolution and spectroscopic contrast in the murine retina. Biomed Optics Express 9:2115–2129; 2018.

Kim WK, Donalson LM, Herrera P, Woodward CL, Kubena LF. Effects of different bone preparation methods (fresh, dry, and fat-free dry) on bone parameters and the correlations between bone breaking strength and the other bone parameters. Poult Sci 83:1663–1666; 2004.

Kononov VN, Bokhovko MV, Kononov OE, Soloviev NA, Chu WT, Nigg D. Accelerator based fast neutron sources for neutron therapy. Nucl Instr Meth Phys Res A 564:525–531; 2006.

Ladd AJ, Kinney JH, Haupt DL, Goldstein SA. Finite-element modeling of trabecular bone: comparison with mechanical testing and determination of tissue modulus. J Orthop Res 16:622–628; 1998.

Lang T, LeBlanc A, Evans H, Lu Y, Genant H, Yu A. Cortical and trabecular bone mineral loss from the spine and hip in long-duration spaceflight. J Bone Miner Res 19:1006–12; 2004.

Lee CL, Zhou XL. Thick target neutron yields for the ^{7}Li(p,n)^{7}Be reaction near threshold. Nuc Instr Meth B 152:1–11; 1998.

Liskien H, Paulsen A. Neutron production cross sections and energies for the reactions ^{7}Li(p,n)^{7}Be and ^{7}Li(p,n)^{7}Be*. At Data Nucl Data Tables 15:57–84; 1975.

Martin JE. Physics for radiation protection: a handbook. GmbH, Germany: Wiley; 2006: 650.

Matysiak W, Prestwich WV, Byun SH. Precise measurements of the thick target neutron yields of the 7Li(p,n) reaction. Nucl Inst Meth Phys Res A 643:47–52; 2011.

Mitchell MJ, Logan PM. Radiation-induced changes in bone. Radiograph 18:1125–1136; 1998.

National Bureau of Standards. Handbook 63. Protection from neutron radiation up to 30 MeV. Gaithersburg, MD: NBS; 1957.

National Council on Radiation Protection and Measurements. Calibration of survey instruments used in radiation protection for the assessment of ionizing radiation fields and radioactive surface contamination. Bethesda, MD: National Council on Radiation Protection and Measurements; Report No. 112; 1997.

National Council on Radiation Protection and Measurements. Radiation protection guidance for activities in low-earth orbit. Bethesda, MD: National Council on Radiation Protection and Measurements; Report No. 132; 2000.

Nyaruba MM, Yamamoto I, Kimura H, Morita R. Bone fragility induced by x-ray irradiation in relation to cortical bone-mineral content. Acta Radiol 39:43–46; 1998.

Pejovic-Milic A, Byun SH, Chettle DR, McNeill FE, Prestwich WV. Development of an irradiation/shielding cavity for in vivo neutron activation analysis of manganese in human bone. J Radioanal Nucl Chem 269:417–420; 2006.

Tochilin E, Ross SW, Shumway BW, Kohler GD, Golden R. Cyclotron neutron and γ-ray dosimetry for animal irradiation studies studies. Rad Res 4:158; 1956.

Wernle JD, Damron TA, Allen MJ, Mann KA. Local irradiation alters bone morphology and increases bone fragility in a mouse model. J Biomech 43:2738–2746; 2010.

Wei F, Neal CJ, Sakthivel TS, Fu Y, Omer M, Adhikary A, Ward S, Ta KM, Moxon S, Molinari M, Asiatico J, Kinzel M, Yarmolenko SN, Cheong VS, Orlovskaya N, Ghosh R, Seal S, Coathup M. A novel approach for the prevention of ionizing radiation-induced bone loss using a designer multifunctional cerium oxide nanozyme. Bioact Materials 21:47–565; 2023.

Wiley JS, Lloyd SAJ, Nelson GA, Bateman TA. Ionizing radiation and bone loss: space exploration and clinical therapy applications. Clin Rev Bone Miner Metab 9:54–62; 2011.

Williams HJ, Davies AM. The effect of x-rays on bone: a pictorial review. Eur Radiol 16:619–633; 2006.

Zinke-Allmang M, Nejat R, Galiano-Riveros E, Bayer J, Chen M. Elasticity and vibrations. In: Physics for the life sciences. Toronto: Nelson Education Ltd.; 2017: 346–351.

■■